Received: 3 August 2023 | Revised: 1 November 2023 | Accepted: 2 November 2023

DOI: 10.1002/jex2.123

RESEARCH ARTICLE

Intracellular localisation and extracellular release of Y RNA and Y RNA binding proteins

Tom A. P. Driedonks[1,2] | **Sarah Ressel**[3] | **Thi Tran Ngoc Minh**[1,4] | **Amy H. Buck**[3] | **Esther N. M. Nolte-'t Hoen**[1]

[1]Department Biomolecular Health Sciences, Fac. Veterinary Medicine, Utrecht University, Utrecht, The Netherlands

[2]Department CDL Research, University Medical Centre Utrecht, Utrecht, The Netherlands

[3]Institute of Immunology & Infection Research, School of Biological Sciences, University of Edinburgh, Edinburgh, UK

[4]Biomolecular Mass Spectrometry and Proteomics, Bijvoet Centre for Biomolecular Research and Utrecht Institute of Pharmaceutical Sciences, Utrecht University, Utrecht, The Netherlands

Correspondence
Tom Driedonks and Esther N.M. Nolte-'t Hoen, Department Biomolecular Health Sciences, Faculty of Veterinary Medicine, Utrecht University, Utrecht, The Netherlands.
Email: tdriedon@umcutrecht.nl and e.n.m.nolte@uu.nl

Funding information
FP7 Ideas: European Research Council, Grant/Award Number: 337581; European Research Council, Grant/Award Number: 101002385

Abstract

Cells can communicate via the release and uptake of extracellular vesicles (EVs), which are nano-sized membrane vesicles that can transfer protein and RNA cargo between cells. EVs contain microRNAs and various other types of non-coding RNA, of which Y RNA is among the most abundant types. Studies on how RNAs and their binding proteins are sorted into EVs have mainly focused on comparing intracellular (cytoplasmic) levels of these RNAs to the extracellular levels in EVs. Besides overall transcriptional levels that may regulate sorting of RNAs into EVs, the process may also be driven by local intracellular changes in RNA/RBP concentrations. Changes in extracellular Y RNA have been linked to cancer and cardiovascular diseases. Although the loading of RNA cargo into EVs is generally thought to be influenced by cellular stimuli and regulated by RNA binding proteins (RBP), little is known about Y RNA shuttling into EVs. We previously reported that immune stimulation alters the levels of Y RNA in EVs independently of cytosolic Y RNA levels. This suggests that Y RNA binding proteins, and/or changes in the local Y RNA concentration at EV biogenesis sites, may affect Y RNA incorporation into EVs. Here, we investigated the subcellular distribution of Y RNA and Y RNA binding proteins in activated and non-activated THP1 macrophages. We demonstrate that Y RNA and its main binding protein Ro60 abundantly co-fractionate in organelles involved in EV biogenesis and in EVs. Cellular activation led to an increase in Y RNA concentration at EV biogenesis sites and this correlated with increased EV-associated levels of Y RNA and Ro60. These results suggest that Y RNA incorporation into EVs may be controlled by local intracellular changes in the concentration of Y RNA and their protein binding partners.

KEYWORDS
exosomes, extracellular vesicles, non-coding RNA, subcellular localisation, TLR activation, Y RNA

1 | INTRODUCTION

Extracellular vesicles (EVs) are ~50–500 nm sized membrane-enclosed vesicles that are released by virtually all cells. EVs are formed either by budding from the plasma membrane ('microvesicles') or through inward budding of the endosomal membrane and fusion of the resulting multivesicular-endosomes with the plasma membrane ('exosomes') (van Niel et al., 2018). EVs play a role in intercellular communication by transferring protein and RNA cargo between cells (de Jong et al., 2020; Ridder et al., 2015; Valadi et al., 2007; Zomer et al., 2015). Various classes of small non-coding RNA (ncRNA) have been detected in EVs (Bellingham

et al., 2012; Nolte-'t Hoen et al., 2012). Of these RNA classes, miRNA have been most intensively investigated because of their well-established modulatory effects on mRNA levels (He & Hannon, 2004). Besides miRNA, EVs contain various other ncRNA classes, such as Y RNA, 7SL (SRP-RNA), tRNA and snRNA (Bellingham et al., 2012; Nolte-'t Hoen et al., 2012). Inside of cells, many of these ncRNAs are known to function as structural components of RNA-protein complexes involved in housekeeping processes, such as mRNA splicing, RNA quality control and protein translation (Akopian et al., 2013; Anderson & Ivanov, 2014; Boccitto & Wolin, 2019; Matera & Wang, 2014). It is largely unknown whether these ncRNA types play additional roles in cell-to-cell signalling via EVs.

Y RNA is one of the most abundant ncRNA types in EVs based on multiple studies using various cell types and body fluids (reviewed in (Driedonks & Nolte-'t Hoen, 2019)). This family of polymerase III transcribed stem-loop RNAs is conserved among mammals (Pruijn et al., 1993), with four Y RNA subtypes in the human genome (Y1, Y3, Y4, Y5) and two subtypes in the mouse genome (Y1 and Y3). In cells, Y RNA serves as a scaffold for several RNA binding proteins (RBPs) and regulates various cellular processes (Köhn et al., 2015; Leng et al., 2020). Ro60 (also known as SSA) and La (also known as SBB) are the most intensely studied Y RNA binding proteins. Binding of Y RNA affects the localisation and activity of its protein partners, while these proteins influence the stability and function of Y RNA. Ro60 binds the stem-motif and is required for cytoplasmic stability of Y RNA (Chen et al., 2003), while La binds the 3′ oligo-uridine motif of Y RNA and protects it from exonucleolytic degradation (Wolin & Cedervall, 2002). Furthermore, La binding shields the 5′ triphosphate nucleotide of Y RNA, which may otherwise activate the innate immune receptor RIG-I (Hornung et al., 2006). Ro60 can shuttle between nucleus and cytoplasm, but is retained in the cytoplasm when Y RNA is bound (Leng et al., 2020; Sim et al., 2009). Furthermore, Y RNA binding to Ro60 prevents the binding of misfolded ncRNAs to its central cavity, thereby regulating RNA degradation (Fuchs et al., 2006; Stein et al., 2005). In addition to these well-studied Y RNA binding proteins, several other RBPs, such as hnRNP K (Fabini et al., 2001), HuR (Scheckel et al., 2016; Tebaldi et al., 2018) and ZBP1 (Sim et al., 2012), interact with the oligopyrimidine loop region of Y RNA, which may regulate their activity or localisation. For example, Y3 RNA can scavenge an enhancer protein, HuD (ELAVL4), away from the 3′UTRs of mRNAs, thereby affecting mRNA translation in the context of neuronal differentiation (Tebaldi et al., 2018).

While Y RNA is one of the most abundant EV-associated ncRNAs, the functions of extracellular Y RNA are not well understood. It is emerging that changes in extracellular Y RNA levels correlate with various diseases and immune-related processes (reviewed in Driedonks and Nolte-'t Hoen (2019)). For example, increased levels of extracellular Y RNA and Y RNA fragments have been reported in the plasma of various types of cancer patients (Dhahbi et al., 2013; Haderk et al., 2017; Lovisa et al., 2020). Additionally, plasma of coronary artery disease patients contained increased levels of Y RNA fragments (Repetto et al., 2015). Furthermore, we have shown that systemic inflammation altered the ratios between Y RNA subtypes in human plasma (Driedonks et al., 2020). Besides these disease-associated changes in extracellular Y RNA levels in plasma, we have shown that cellular activation in vitro changed the incorporation of Y RNA into EVs (Driedonks et al., 2018). These data indicate a relation between the activation/differentiation/transformation status of cells and Y RNA release via EVs. However, how environmental stimuli or disease status impact Y RNA incorporation into EVs and their extracellular release is largely unknown.

A large number of studies have addressed how ncRNA types other than Y RNA, mainly miRNAs, are incorporated into EVs. It is known that changes in the cytoplasmic abundance of ncRNAs influence their incorporation into EVs (Gámbaro et al., 2019). Additionally, several different RBPs have been suggested to regulate incorporation of specific miRNAs into EVs (Cha et al., 2015; Lee et al., 2019; Mukherjee et al., 2016; Santangelo et al., 2016; Shurtleff et al., 2016; Statello et al., 2018; Temoche-Diaz et al., 2019; Villarroya-Beltri et al., 2013), presumably by recruiting these miRNAs to EV biogenesis sites, such as multivesicular endosomes (MVE) (Mateescu et al., 2017). Other proteins, such as hnRNP U, may selectively retain specific miRNAs in cells (Zietzer et al., 2020). Much less is known about how incorporation of the other (non-miRNA) classes of extracellular RNA is regulated. In one study, knockout of the RNA binding protein YBX1 decreased the incorporation of Y RNA and tRNA in CD63-positive EVs, while increasing cellular levels of Y RNA and tRNA (Shurtleff et al., 2017). Furthermore, we previously reported that activation of immune cells changed the abundance of EV-associated Y RNA independently of cellular Y RNA levels (Driedonks et al., 2018). This suggests that Y RNA binding proteins, and/or changes in the local Y RNA concentration at cellular compartments where EVs are formed, may regulate the incorporation of Y RNA into EVs.

Here, we aimed to connect activation-induced extracellular release of Y RNA in EVs to its intracellular localisation. We determined the subcellular distribution of Y RNA and Y RNA binding proteins, and assessed how cellular activation affects the abundance of Y RNA and/or Y RNA binding proteins in cellular compartments involved in EV biogenesis. We used THP1 macrophages, stimulated or not with a Toll-like receptor (TLR) 1/2 agonist, and employed a subcellular fractionation protocol that enabled parallel quantification of both proteins and ncRNA in various cellular organelles. We demonstrate that Y RNA and its main binding protein Ro60 abundantly co-fractionate in organelles involved in EV biogenesis and in EVs in a cell activation-dependent manner. The results suggest that Y RNA incorporation into EVs may be controlled intracellularly by local changes in the concentration of Y RNA.

2 | MATERIALS AND METHODS

2.1 | Cells and EV production

The human monocytic cell line THP1 was a kind gift from M. Boes at UMC Utrecht and was maintained in IMDM (Gibco, Paisley, UK) supplemented with 10% FCS (Bodinco, Alkmaar, The Netherlands), 2 mM ultraglutamine and 100 U/mL penicillin/streptomycin (Gibco, Paisley, UK). EV-depleted medium was prepared as described previously (Driedonks et al., 2018). In brief, FCS was pre-diluted to 30% in IMDM and ultracentrifuged at 100,000 × *g* in a SW28 rotor overnight (k-factor 334.2). EV-depleted FCS was pipetted from the ultracentrifuge tubes and used at 10% final concentration in IMDM, supplemented with 2 mM ultraglutamine and 100 U/mL pen/strep. Cells were sub-cultured by dilution twice per week. For all experiments, cells were seeded at 0.5 million cells/mL. The time-course experiment was done in 6-well dishes, all other experiments were done in T75 and T175 flasks. Cells were differentiated into a macrophage phenotype by treatment with 10 ng/mL phorbol-12-myristate-13-acetate (PMA, Sigma, St. Louis, MO) for 24 h. Medium was removed, after which cells were washed with 3 mL PBS (Gibco, Paisley, UK) and replenished with EV-depleted medium. Where indicated, cells were stimulated with 5 μg/mL Pam3CSK4 (EMC Microcollections, Tübingen, Germany). Subcellular fractionation was done after 4 h of culture, the culturing times of the time course experiment are indicated in Figure 1g. Cells were cultured for 20–24 h for EV production. Viability of cells was checked by Trypan Blue (Sigma, Sigma, St. Louis, MO) exclusion and was above 95% for all experiments.

2.2 | EV purification

EVs were purified by differential ultracentrifugation as described before (Driedonks et al., 2018). In brief, supernatant was collected and centrifuged at 4°C for 2 × 10 min at 200 × *g*, 2 × 10 min at 500 × *g* and 1 × 30 min at 10,000 × *g*. Supernatant was carefully removed by pipetting, not disturbing the 10,000 × *g* pellet, and EVs were pelleted from this supernatant by centrifugation at 100,000 × g_{max} for 65 min in a SW28 (k-factor 334.2) or SW40 (k-factor 280.3) rotor. EV pellets were resuspended in 20 μL PBS + 0.2% BSA (previously depleted of particles by overnight centrifugation at 100,000 × g_{max}), and labelled with 1.5 μL fluorescent dye PKH67 in 100 μL diluent C (Sigma, St. Louis, MO). Labelled EVs were mixed with 2.5 M sucrose, overlaid with a sucrose density gradient (2.0–0.4 M sucrose in PBS) and centrifuged 15–18 h at 192,000 × g_{avg} in a SW40 rotor (k-factor 144.5). The densities of sucrose fractions were determined by measuring 10 μL of each fraction on an Abbe refractometer (Atago, Japan). EVs in sucrose fractions were quantified using high-resolution flow cytometry, or were pelleted from the fractions with densities of 1.11–1.18 g/mL by dilution in PBS + 0.2% BSA followed by centrifugation for 65 min at 192,000 × g_{avg} in a SW40 rotor (k-factor 144.5).

2.3 | High-resolution flow-cytometry

Sucrose density fractions were diluted 20x in PBS just before flow-cytometric quantification on a BD Influx (BD Biosciences, San Jose, CA) with an optimised configuration for small particle detection (Nolte-'t Hoen et al., 2012; van der Vlist et al., 2012). In brief, fluorescence based threshold triggering was applied, and forward-scatter (FSC) was detected at a 15–25 degree collection angle. Fluorescent 100 and 200 nm polystyrene beads (Fluospheres, Invitrogen, Carlsbad, CA) were used to calibrate the instrument before measurement. Fluorescent events were collected in a 30 s timeframe for all samples and were measured at event rates below 10,000 events/s, which is below the limit of the electronic pulse processing of the BD Influx (Groot Kormelink et al., 2016). Thus, relative EV concentrations were defined as 'events per 30 seconds'.

2.4 | Subcellular fractionation

For the time course experiment, stimulated and unstimulated cells were washed and detached with PBS + 2 mM EDTA at the timepoints indicated in Figure 1g. Cells were pelleted 1 min at 10,000 × *g*, lysed in 50 μL PBS + 1% Triton-X100 for 5 min on ice, after which nuclei were spun down 5 min at 16,000 × *g* at 4°C. Supernatant was collected, centrifuged again to remove any residual nuclei, mixed with 700 μL Qiazol and stored at −80°C until RNA isolation.

Subcellular fractionation was performed using a protocol based on Gibbings (2011) and Gibbings et al. (2009). Four hours after activation with Pam3CSK4, cells were harvested from flasks using a rubber cell scraper. Five million cells per condition were pelleted at 200 × *g* for 10 min at 4°C, washed in ice-cold PBS and incubated for 10 min in ice-cold hypotonic homogenisation buffer (0.083 M sucrose, 10 mM HEPES, 1 mM EGTA) supplemented with the following inhibitors: Complete Mini protease inhibitor cocktail (Roche, Basel, Switzerland), 200 μM MG132 proteasome inhibitor (Calbiochem, Darmstadt Germany), 8 mM vanadyl

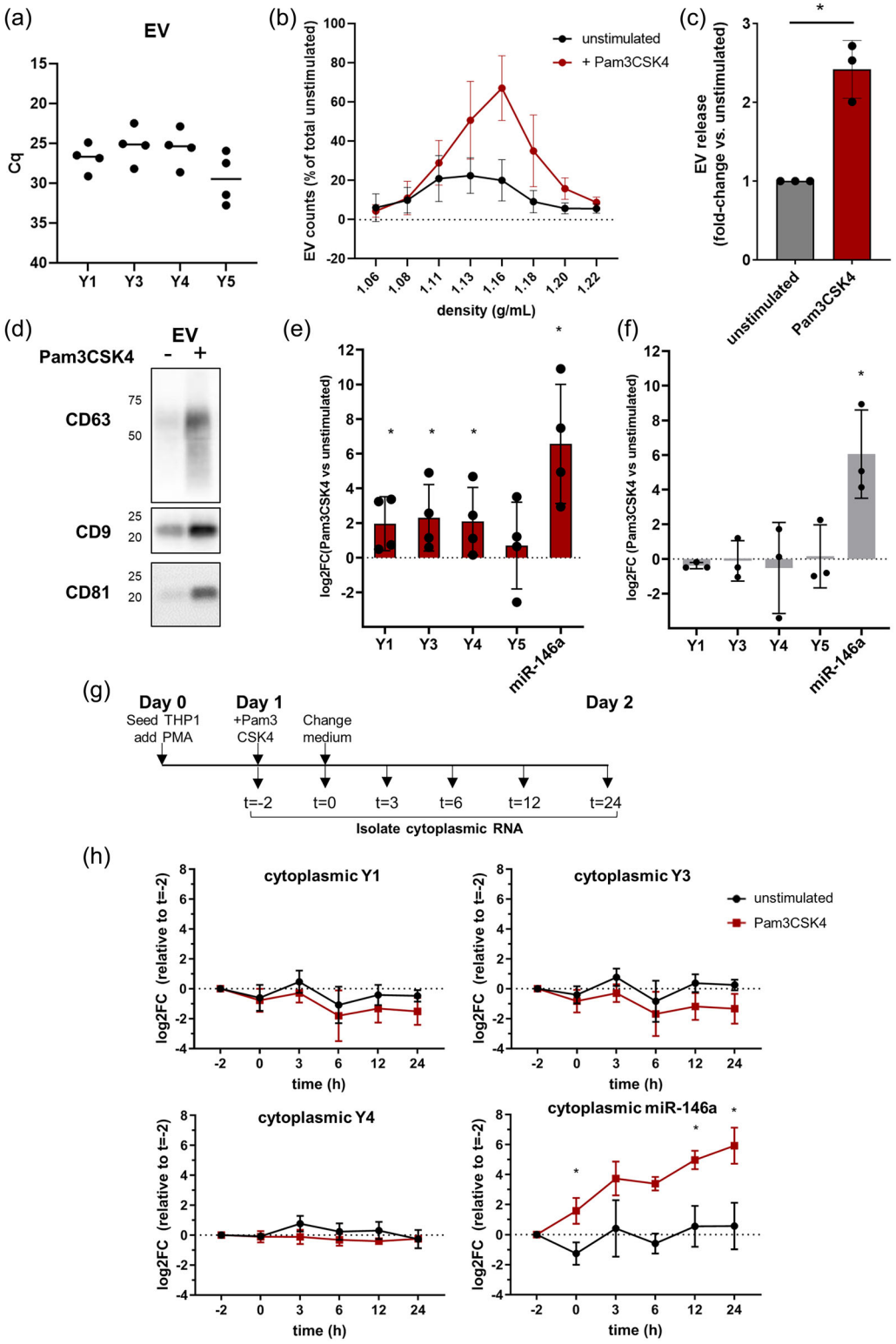

FIGURE 1 Pam3CSK4 stimulation of THP1 cells increases the release of EV-associated Y RNA. THP1 macrophages cultured in EV-depleted medium were stimulated with Pam3CSK4 or left unstimulated. After overnight incubation, EVs were purified by differential ultracentrifugation, labelled with PKH67 fluorescent dye, and floated into a sucrose density gradient. (a) Y RNA subtypes were quantified by RT-qPCR in EVs (fractions 1.11–1.18 g/mL) released by unstimulated THP1 cells, $n = 4$ experiments. No significant differences in Y RNA subtype abundance, one-way ANOVA with Tukey's post-hoc test. (b) High resolution flow cytometry based quantification of EVs in the different sucrose density fractions. EV concentration in each fraction was measured in a 30 s timeframe, expressed as 'EV counts / 30 sec'. Event counts in each fraction were normalised to the total number of events in all fractions of the unstimulated condition. Data from $n = 3$ experiments. (c) Relative difference in EV numbers (fractions 1.11–1.18 g/mL) released by unstimulated and Pam3CSK-stimulated

(Continues)

FIGURE 1 (Continued)

THP1 cells. *$p < 0.05$, Student's paired t test, two tailed, $n = 3$ experiments. (d) Western blot analysis of EVs isolated from equal numbers of stimulated and unstimulated THP1 cells, representative for $n = 4$ (CD9) or $n = 2$ (CD81 and CD63) experiments. (e) RT-qPCR quantification of Y RNA subtypes and endotoxin responsive miR-146a in equal amounts of EV RNA released in 24 h under stimulated/unstimulated conditions. Data are shown as log2 fold differences, using U6 RNA levels for normalisation. *$p < 0.05$, Student's paired t test, two tailed, $n = 4$ experiments. (f) RT-qPCR quantification of Y RNA subtypes and endotoxin responsive miR-146a in intracellular RNA in stimulated/unstimulated conditions. Data are shown as log2 fold differences, using U6 RNA levels for normalisation. *$p < 0.05$, Student's paired t test, two tailed, $n = 3$ experiments. (g) Schematic overview of time course experiment. THP1 macrophages were stimulated with Pam3CSK4 or left untreated. Two hours later ($t = 0$), culture medium was exchanged for EV depleted medium, cytoplasmic RNA was isolated at the indicated time points. (h) RT-qPCR based quantification of cytoplasmic Y RNA subtypes and miR-146a during the time course. Log2 fold changes in RNA expression were calculated relative to the RNA abundance at the beginning of the time course ($t = -2$). Black line: unstimulated, red line: Pam3CSK4 stimulated. *$p < 0.05$, Student's paired t test, two-tailed, $n = 3$ independent experiments.

ribonucleoside (New England Biolabs, Ipswitch, MA), 8 μL RNAse Out (Invitrogen, Carlsbad, CA). Cells were homogenised by 40 passages through a 26G needle using a 1 mL syringe. Trypan blue exclusion was performed on the homogenates to ensure comparable numbers of cells were disrupted, typically >95%. Nuclei and large cell debris were removed by centrifugation for 5 min at 1000 × g at 4°C, after which the supernatant was subjected to a second centrifugation step to ensure all debris was removed. The supernatant (post-nuclear cytosolic fraction) was loaded on top of a 5%–40% Optiprep (Axis-Shield, Dundee, UK) gradient in 78 mM KCl, 4 mM $MgCl_2$, 8.4 mM $CaCl_2$, 10 mM EGTA, 50 mM HEPES-NaOH pH 7.0 prepared in SW60 tubes. Tubes were spun in a SW60 rotor at 100,000 × g_{avg} (32,000 rpm k-factor 159.6) for 18–20 h at 4°C to separate the subcellular organelles according to their buoyant density. Subsequently, 300 μL fractions were collected. The densities of sucrose fractions were determined by measuring 10 μL of each fraction on an Abbe refractometer (Atago, Japan). Of these fractions 50 μL aliquots were pooled for RNA isolation (fractions 1+2+3, 4+5, 6+7, 8+9 and 10+11+12). The remaining 250 μL was pooled for TCA precipitation using the following protocol: sodium-deoxycholate (Sigma, St. Louis, MO) was added to the fractions at 125 μg/mL, after which 10% tricholoroacetic acid (final concentration) was added. Samples were incubated on ice for 15 min, protein precipitates were pelleted for 10 min at 16,000 × g at 4°C. Supernatant was removed gently, after which 0.5 mL −20°C acetone was added to the pellets. Samples were incubated at −20°C for 10 min followed by centrifugation for 10 min at 16,000 × g at 4°C. Supernatant was removed and 0.5 mL −20°C acetone was added to the pellets followed by centrifugation for 10 min at 16,000 × g at 4°C to wash. Supernatant was taken off, pellets were left to dry to the air until all acetone had evaporated. Pellets were resuspended in 30 μL 2x SDS sample buffer and 5 μL 1 M Tris pH 8.8 was added to adjust the pH.

2.5 | Western blot

Protein samples were denatured for 3 min at 100°C in 2x SDS sample buffer and separated on a 10% SDS-PAGE gel, followed by protein transfer onto 0.45 μm Immobilon-P PVDF membranes (Millipore, Cork, Ireland). After blocking for >1 h in blocking buffer (0.5% Cold Fish Skin Gelatin (Sigma-Aldrich, St. Louis, MO) in PBS + 0.05% Tween-20), blots were incubated overnight at 4°C with primary antibodies rabbit-anti-YBX1 (Cell Signaling, 4202, 1:1000), rabbit-anti-Lamp-1 (SantaCruz, sc-5571, 1:1000), mouse-anti-hnRNP K (SantaCruz, sc-28380, 1:5000), mouse-anti-Calnexin (Transduction Labs, clone 37, 1:1000), mouse-anti-HuR (SantaCruz, sc-5261, 1:1000), mouse-anti-Ro60 (a kind gift from S.L. Wolin, 1:50), rabbit-anti-La (Cell Signaling, 5034, 1:1000), mouse-anti-CD9 (BioLegend, HI9a, 1:1000), mouse-anti-CD63 (Abcam, ab59479, 1:1000), rabbit-anti-Histone-H3 (Cell Signaling, 9715, 1:1000), mouse-anti-CD81 (SantaCruz, clone B-11, 1:1000) in blocking buffer. Blots were washed and incubated for 1–2 h with HRP-coupled secondary antibodies (Dako, cat P0450 and P0448, 1:5000). ECL solution (ThermoScientific, SuperSignal West Dura Extended Duration Substrate, cat. 34075) was used for detection on a Chemidoc imager (BioRad, Hercules, CA). Images were analyzed by Image Lab software (BioRad, Hercules, CA).

2.6 | RNA isolation, cDNA synthesis and RT-qPCR

mRNA was isolated from cell pellets 4 h after stimulation using the Nucleospin RNA kit (Macherey-Nagel, Düren, Germany) according to the manufacturer's instructions, including DNase treatment. cDNA was prepared using the RevertAid cDNA kit (ThermoScientific) following the manufacturer's instructions and using random hexamer primers.

Small ncRNA was isolated from pelleted cells, EVs, or from pooled subcellular fractions using the miRNeasy micro kit (Qiagen, Hilden, Germany). 700 μL Qiazol was added to pellets or to 150 μL pooled Optiprep fractions, after which the manufacturer's instructions were followed. Quantification of the eluted RNA was done by Bioanalyzer Pico 6000 (Agilent, Waldbronn, Germany). cDNA synthesis was done using the miScript RT II kit (Qiagen, Hilden, Germany) using HiFlex buffer, according to the manufacturer's instructions, RNA input was normalised according to the concentration of 20–300 nt small RNA. For qPCR, cDNA was pre-diluted 10x in MQ water, and 2 μL diluted cDNA template was used for amplification of target RNAs with 0.8 μM

TABLE 1 PCR primers used in this study.

No	Primer name	Sequence (5′–3′)
1	Y1 loop-F	GATCGAACTCCTTGTTCTACTC
2	Y3 loop-F	AGATTTCTTTGTTCCTTCTCCACTC
3	Y4 loop-F	GTGTCACTAAAGTTGGTATACAAC
4	Y5 loop-F	GTTAAGTTGATTTAACATTGTCTC
5	miR-146a	TGAGAACTGAATTCCATGGGT
6	U6-F	CTCGCTTCGGCAGCACA
7	7SL-F	GGAGTTCTGGGCTGTAGTGC
8	Y RNA fl-F	GGCTGGTCCGATGGTAGTG
9	Y RNA fl-R	AAAGCCAGTCAAATTTAGCAGTG
10	5S-F	TCTACGGCCATACCACCCTGA
11	5S-R	GCCTACAGCACCCGGTATTCC
12	18S-F	CGCGGTTCTATTTTGTTGGT
13	18S-R	AGTCGGCATCGTTTATGGTT
14	hActin-F	CCTTCCTGGGCATGGAGTCCTG
15	hActin-R	GGAGCAATGATCTTGATCTTC
16	hIL-6-F	AACCTGAACCTTCCAAAGATGG
17	hIL-6-R	TCTGGCTTGTTCCTCACTACT
18	hTNFa-F	ATGAGCACTGAAAGCATGATCC
19	hTNFa-R	GAGGGCTGATTAGAGAGAGGTC

TABLE 2 Northern blot oligos used in this study.

No	Primer name	Sequence (5′–3′)
1	Y1_loop_compl	GGGGGGAAAGAGTAGAACAAGGAGTTCG
2	Y3_loop_compl	GCAGTGGGAGTGGAGAAGGAACAAAG
3	Y4_loop_compl	GGGGGGTTGTATACCAACTTTAGTGACAC
4	5S	AAG CCT ACA GCA CCC GGT ATT C

primers (IDT, Leuven, Belgium) in SensiMix PCR master mix (BioLine, UK). The following PCR program was used for amplification of mRNA: 95°C 10 min, followed by 40 cycles of 10 s at 95°C, 20 s at 60°C and 45 s at 72°C. For small RNA we used the following PCR program: 95°C 10 min, followed by 50 cycles of 10 s at 95°C, 20 s at 57°C and 30 s at 72°C. Melt curves were run from 65 to 95°C after each PCR. All qPCRs were performed on a Biorad CFX96 or CFX384 machine (BioRad, Hercules, CA). Normalisation of small RNA qPCR data was done relative to U6 snRNA in line with earlier studies (Squadrito et al., 2014, Driedonks et al., 2018), and to beta-actin for mRNA qPCR data.

The following PCR primers were used (Table 1). Primers 1–7 were used in combination with the miScript universal reverse primer, primers 8–19 were used as pairs of specific forward and reverse primers:

2.7 | Northern blot

Total cellular RNA or RNA from subcellular fractions (6–10 ng per lane) was denatured in gel loading buffer II (Invitrogen) for 2 min at 70°C and snap-cooled on ice before loading on a denaturing 10% PAGE gel (National Diagnostics, Nottingham, United Kingdom), run for 1.5 h at 125 V. RNA was transferred onto a Hybond-N Nylon membrane (Amersham Pharmacia Biotech, GE Healthcare Bio-Sciences, Pasching, Austria) and chemically crosslinked with 1-ethyl-3-(3-dimethylaminopropyl) carbodimide (Sigma) at 55°C for 2 h (Pall & Hamilton, 2008). ^{32}P-labelled DNA oligo probes perfectly complementary to specific regions of each RNA species (Table 2) were hybridised overnight at 42°C in PerfectHyb (Sigma) solution. Blots were analysed by phosphorimaging using a Typhoon Scanner (GE Healthcare).

2.8 | Microscopy

Microscopic images were taken on an Olympus CK2 light microscope with a Leica camera at 200x magnification.

2.9 | Statistical analysis

Statistical analyses (One-way ANOVA, Student's *t* test, paired t test, or one sample *t* test, as indicated in the Figure legends), were done in SPSS v24, p-values <0.05 were considered statistically significant.

2.10 | Data availability

We have submitted all relevant data of our experiments to the EV-TRACK knowledgebase (EV-TRACK ID: EV210336) (Van Deun et al., 2017).

3 | RESULTS

3.1 | EV-associated Y RNA levels are affected by stimulation of THP1 macrophages

We first confirmed the presence of Y RNA subtypes in EVs released by macrophage-differentiated THP1 cells. EVs were isolated from culture supernatant by sucrose density gradient centrifugation, and subjected to RNA isolation. We used primers directed against the variable loop region of Y RNA (Driedonks et al., 2020) to specifically detect Y RNA subtypes Y1, Y3, Y4 and Y5 by RT-qPCR (Figure 1a). Y RNA subtypes Y1, Y3 and Y4 were more abundantly detected in EVs than Y5, consistent with previous publications (reviewed in (Driedonks & Nolte-'t Hoen, 2019)), but did not reach significance. Our previous work revealed that immune activation changed Y RNA levels in EVs from mouse dendritic cells (Driedonks et al., 2018). Here, we investigated whether activation of human THP1-derived macrophages cells would also change the release of EV-associated Y RNA. THP1 macrophages were stimulated with TLR2/1 ligand Pam3CSK4, and their activated phenotype was confirmed based on morphological changes (van Helden et al., 2008) (Figure S1A) and increased production of the inflammatory cytokines IL-6 and TNFα (Figure S1B). Pam3CSK4-stimulated cells released over twofold more EVs than unstimulated cells, as measured by high-resolution flow cytometry, while their buoyant density was comparable (Figure 1b,c). In line with the higher number of EVs, increased amounts of the common EV-associated proteins CD9, CD63 and CD81 were detected in EV isolates of Pam3CSK4-stimulated cells (Figure 1d,e). EVs from Pam3CSK4-stimulated THP-1 macrophages contained increased amounts of Y1, Y3 and Y4 relative to the total EV RNA input, while stimulation did not affect intracellular Y RNA levels (Figure 1e,f). This was different from the levels of miR-146a, which were upregulated in both cells and EVs, as also shown previously (Driedonks et al., 2018; Taganov et al., 2006). These data indicate that EV-associated levels of Y1, Y3 and Y4, but not Y5, are affected by cell-activating stimuli. The lack of activation-induced effects on intracellular abundance suggests that the incorporation of these Y RNA subtypes into EVs is regulated by a cellular sorting process. We next aimed to exclude that the observed increase in EV-associated Y1, Y3 and Y4 after TLR stimulation was caused by a transient upregulation in cytoplasmic Y RNA, which could occur shortly after activation and be resolved through Y RNA release via EVs. We isolated cytoplasmic RNA at different timepoints after activation (Figure 1g), and quantified the levels of Y1, Y3 and Y4 and miR-146a (control) by RT-qPCR (Figure 1h). Throughout the time course, cytoplasmic Y RNA levels did not significantly change in response to Pam3CSK4-stimulation, in line with Figure 1f. In contrast, the cytoplasmic levels of miR-146a were significantly increased at timepoint zero (2 h after activation), and increased steadily for the following 24 h (in line with (Mann et al., 2017; Taganov et al., 2006)). The increase in cytoplasmic miR-146a levels was similar to the increase observed in EVs isolated after 20–24 h (Figure 1e). Thus, activation-dependent changes in EV-associated Y1, Y3 and Y4 RNA cannot be explained by changes in their cytoplasmic abundance. Based on these data we considered the TLR-stimulated THP1 cells as a suitable model system to further investigate shuttling of Y1, Y3 and Y4 into EVs.

3.2 | Subcellular fractionation allows parallel quantification of RNA and RNA binding proteins

Incorporation of specific RNAs into EVs is thought to mediated by RNA binding proteins (RBPs) that may recruit RNAs to sites of EV biogenesis (Mateescu et al., 2017; van Niel et al., 2018). To study whether Y RNA and Y RNA binding proteins are abundantly present at sites of EV biogenesis, we set up a method that allows parallel analysis of RNA and RNA-binding proteins in cellular organelles, adapted from Gibbings (2011) and Gibbings et al. (2009). This method separates cytosolic organelles by density

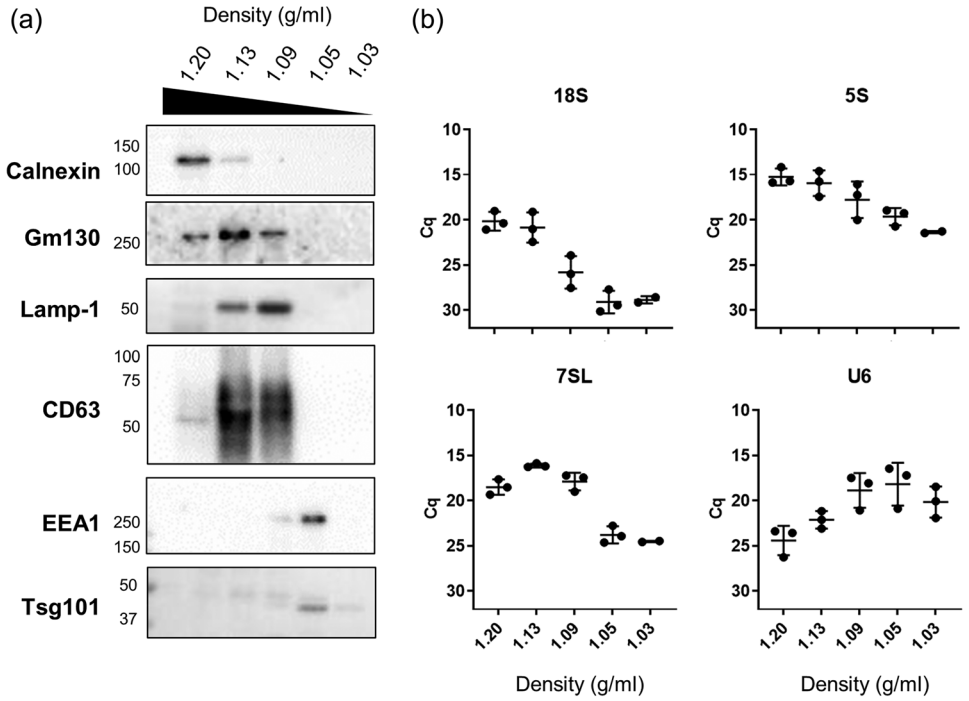

FIGURE 2 Subcellular fractionation reveals the distribution of ncRNA species over different organelle fractions. Organelles of unstimulated THP1 macrophages were separated on an Optiprep density gradient and analyzed by Western blot and RT-qPCR. (a) Western blot detection of protein markers for ER (Calnexin), Golgi (Gm130), lysosomal/late endosomal (Lamp-1, CD63) and endosomal compartments (EEA1, Tsg101). (b) RT-qPCR based detection of small non-coding RNAs 18S, 5S, 7SL and U6 in the distinct density fractions. Data from $n = 3$ experiments are shown.

gradient centrifugation, followed by downstream analysis of both proteins and RNA. We first validated the subcellular distribution of various organelle-specific proteins and RNAs. Post-nuclear cytosol of unstimulated THP1 macrophages, devoid of nuclear protein Histone H3 (Figure S2A), was fractionated overnight on a 5%−40% Optiprep gradient. The different density fractions were analysed for the presence of marker proteins for endoplasmic reticulum (ER), Golgi apparatus, early endosomes, and multivesicular endosome (MVE) (Figures 2a and S3). The ER-associated protein Calnexin and Golgi marker Gm130 were detected in high-density fractions. The endolysosome-associated proteins CD63 and Lamp-1 (Huotari & Helenius, 2011; Kobayashi et al., 2013) were enriched in intermediate density fractions, consistent with earlier reports (Huotari et al., 2012; Squadrito et al., 2014). The endosomal markers EEA1 and Tsg101 (ESCRT-I) were expectedly enriched in low density fractions (Huotari et al., 2012; McKenzie et al., 2016). Small cytosolic proteins not associated to membrane-bound organelles likely remained in the least dense fraction (1.03 g/mL). Next, we evaluated the presence of specific ncRNA types known to be associated with the different organelles. Bioanalyzer measurement indicated that peaks of large ribosomal RNAs (18S and 28S) were most abundant in the high-density fractions (1.20–1.13 g/mL), while most small RNAs were found in intermediate and low-density fractions (<1.09 g/mL) (Figure S2B). By RT-qPCR analysis (Figure 2b), we confirmed that the ribosomal 18S RNA, which is often excluded from EVs, was mainly present in the high-density ER fractions. The ribosomal 5S RNA and the signal-recognition particle complex associated 7SL-RNA (Akopian et al., 2013), which are associated to ribosomes but are often detected in EVs, were present in both the ER and MVE fractions. Small nuclear RNA U6 was predominantly detected in the lighter fractions enriched in endosomal and endolysosomal markers. Besides its predominant nuclear localisation, this snRNA has been detected in cytoplasmic RNP complexes called U-bodies (Liu & Gall, 2007), and is abundantly present in EVs (Crossland et al., 2016; Driedonks et al., 2018; Lässer et al., 2017; Mosbach et al., 2021; Nolte-'t Hoen et al., 2012; Tosar et al., 2015). These data confirmed that our fractionation approach separates organelles and associated ncRNAs to distinct density fractions. Moreover, this confirmed that RNA types known to be present in EVs co-fractionated with MVE markers. This can be either due to their presence in intraluminal vesicles or because the RNAs have been recruited to the limiting membrane of these compartments. This confirmed the suitability of our method to study intracellular sorting of RNAs and RBPs at endosomal compartments in relation to RNAs and RBPs incorporated into released EVs.

3.3 | The presence of Y RNAs and Y RNA binding proteins in subcellular compartments and EVs

Next, we determined the distribution of Y RNA over the subcellular fractions. We quantified the abundance of Y RNA using primers against the 5′ and 3′ stem regions to detect all Y RNA, and primers against the variable loop regions to detect individual

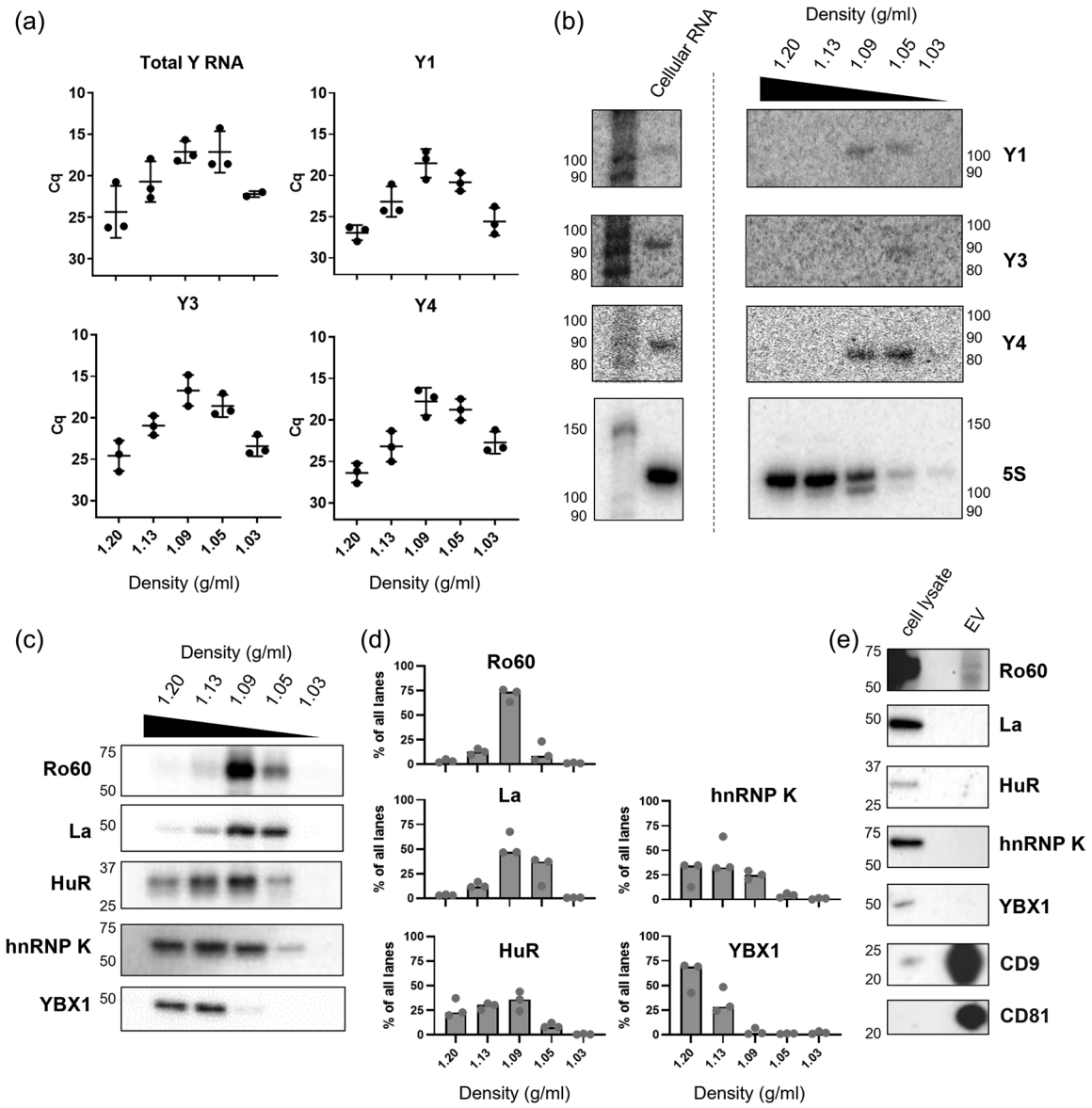

FIGURE 3 Detection of Y RNA and Y RNA binding proteins in subcellular compartments and EVs. Organelles of unstimulated THP1 macrophages were separated on an Optiprep density gradient and analysed by Western blot, RT-qPCR and Northern blot. (a) RT-qPCR based quantification of total Y RNA and individual Y RNA subtypes in the distinct density fractions. Data from $n = 3$ experiments are shown. (b) Northern blot validation of the RT-qPCR data from (a), using 10 ng of RNA per lane. Detection with Y RNA loop probes and 5S probe. Ladder indicates RNA band sizes in lanes containing cellular RNA and subcellular fractions. (c) Y RNA binding proteins Ro60, La, HuR, hnRNP K and YBX1 were detected in the different subcellular fractions by Western blot. Data are representative of $n = 3$ independent experiments. (d) Quantification of band intensities from (a). The relative abundance of each protein was calculated as a percentage of the total band intensity over all fractions per condition. Data from $n = 3$ experiments are shown. (e) EVs were purified from the conditioned supernatant of unstimulated THP1 cells by density gradient centrifugation. Western blot analysis was performed for Y RNA binding proteins Ro60, La, HuR, hnRNP K and YBX1, as well as for the EV-enriched proteins CD9 and CD81. Cell lysates were run alongside as positive control. Data are representative for $n = 3$ experiments.

Y1, Y3 and Y4 subtypes (Figure 3a). Y RNA was most abundantly detected in the fractions enriched in Lamp-1/CD63 (1.09 g/mL), and in Tsg101/EEA1 (1.05 g/mL). Y1, Y3 and Y4 subtypes were similarly distributed over the fractions. The distribution of Y RNAs differed from the distribution of endotoxin responsive miR-146a, which spread more equally over the different fractions and was relatively low in abundance (Figure S2C). We validated the distribution of Y RNA subtypes Y1, Y3 and Y4 in the subcellular fractions by Northern blot (Figure 3b and S4). In agreement with our RT-qPCR data, full-length Y1, Y3, and Y4 were predominantly detected in the 1.05–1.09 g/mL endolysosomal fractions, whereas 5S, included as a control, was predominantly detected in high-density fractions. Additionally, smaller-sized bands of 45–70 nt were observed in fraction 1.09 g/mL (Figure S4), which might be lysosomal Y RNA degradation products. These results indicate that Y RNAs are associated to membranous compartments in the cytosol and co-fractionate with early and late endosomal compartments.

To identify candidate proteins that may facilitate Y RNA sorting into EVs, we assessed the distribution of Y RNA binding proteins in the subcellular fractions. We selected Y RNA binding proteins that were previously detected in EVs by western blotting: Ro60, La, hnRNP K, YBX1 and HuR (Driedonks & Nolte-'t Hoen, 2019). First, we assessed which of these Y RNA binding proteins co-fractionated with Y RNA (Figures 3c,d and S3). The distribution of Ro60 and La overlapped with the distribution of Y RNAs and showed strong enrichment in the endolysosomal fractions. These proteins had a distinct localisation pattern compared to HuR and hnRNP K, which fractionated primarily between the 1.20–1.09 g/mL density range, partly co-fractionating with Y RNAs. In contrast, YBX1 was predominantly found in high density fractions and did not overlap with Y RNA. Overall, these data indicated that Y RNAs and the Y RNA binding proteins Ro60, La, HuR and hnRNP K (partly) co-fractionated with the endosomal/MVE-proteins CD63 and Tsg101. This suggests that Y RNAs and several of their protein binding partners may localise to endosomal sites of EV biogenesis. Next, we assessed by western blot which of the Y RNA binding proteins were incorporated into EVs, using cytosolic cell lysates as positive controls (Figure 3e). While all of the selected Y RNA binding proteins were abundantly detected in cell lysates, only Ro60 was detected in EVs. Even at longer exposure times, up to 50 min, La, HuR, hnRNP K and YBX1 could not be detected in EVs (Figure S5). Thus, both Y RNA and Ro60 were incorporated into EVs, while other Y RNA binding proteins were not, or to a much lesser extent. The observed high abundance of both Y RNA and Ro60 at sites of EV biogenesis may underlie their incorporation into EVs.

3.4 | Stimulation of THP1 cells increases the local Y RNA concentration at EV biogenesis sites

We hypothesised that changes in the local Y RNA concentration at EV biogenesis sites may influence the incorporation of Y RNA into EVs. To test this, we compared the relative abundance of Y RNA in subcellular fractions of THP1 macrophages four hours after stimulation. We first confirmed that TLR activation did not affect the distribution of the organelle markers over the fractions (Figure S6A-B). Next, we quantified the relative abundance of Y RNA subtypes, and miR-146a, in the subcellular fractions of stimulated or non-stimulated cells (Figure 4a). Indeed, we observed a small enrichment of Y1 and Y3 in the 1.05 g/mL fraction during stimulation. In contrast, miR-146a was robustly upregulated in all subcellular fractions of activated cells, most prominently in the lowest density fractions (1.03–1.05 g/mL). We then tested whether the local change in intracellular Y RNA concentration coincided with changes in the amount of Y RNA binding proteins in the different organelle fractions and EVs (Figure 4b,c). The amounts of Ro60 and other Y RNA binding proteins in the subcellular fractions were not significantly altered in response to TLR stimulation. Then, we assessed whether the increase in EV-associated Y RNA coincided with an increase in EV-associated Y RNA binding proteins. Y RNA binding proteins were quantified in isolates containing equal numbers of EVs (particle counts were normalised based on high-resolution flow cytometry data; Figure 1c). We detected an increased amount of Ro60 in EVs from Pam3CSK4-stimulated cells (Figure 4d,e) while CD9, used as loading control, confirmed that equal EV amounts were loaded. The other Y RNA binding proteins could not be detected in EVs upon cell stimulation, as observed previously (Figure 3e). Thus, cellular activation increased the amount of Ro60 and Y RNA per EV. This corresponded with increased local Y RNA concentrations in fractions that contained EV biogenesis markers, suggesting that the local Y RNA concentration may influence its incorporation efficiency.

4 | DISCUSSION

We used parallel analysis of RNA and RBP in fractionated cellular organelles and EVs to study the intracellular sorting of Y RNA and proteins involved in recruitment of Y RNA into EVs. With this biochemical approach, we have shown that the distribution of cytoplasmic Y RNA over subcellular fractions differs from that of other small ncRNA types such as 5S and specific miRNAs. We observed that cytoplasmic Y RNA co-fractionated with specific organelles that were enriched for proteins with known involvement in EV biogenesis. Furthermore, we have shown that various Y RNA binding proteins co-fractionated with these organelles. Of these proteins, Ro60 was the only Y RNA binding protein that was detectably incorporated into EVs. Cellular activation, induced by TLR-stimulation, increased EV-associated Y RNA levels. This increase in extracellular Y RNA release coincided with increased Y RNA abundance in a fraction enriched for endosomal markers Tsg101 and EEA1, suggesting that the local concentration of Y RNA in EV-generating compartments may drive its incorporation into EVs.

4.1 | Subcellular localisation of Y RNA may regulate its incorporation in EVs

To date, the localisation of Y RNA has mainly been studied in terms of its distribution between the nucleus and cytosol (Matera et al., 1995; Sim et al., 2009; Simons et al., 1996). Ro60 is required for nucleo-cytoplasmic translocation of Y RNA (Simons et al., 1996), and for stabilisation of Y RNA in the cytosol (Labbé et al., 1999; Xue et al., 2003). In line with these findings, Y RNA and Ro60 have been observed in close proximity in the cytosol by electron microscopy (Farris et al., 1997). To further delineate the

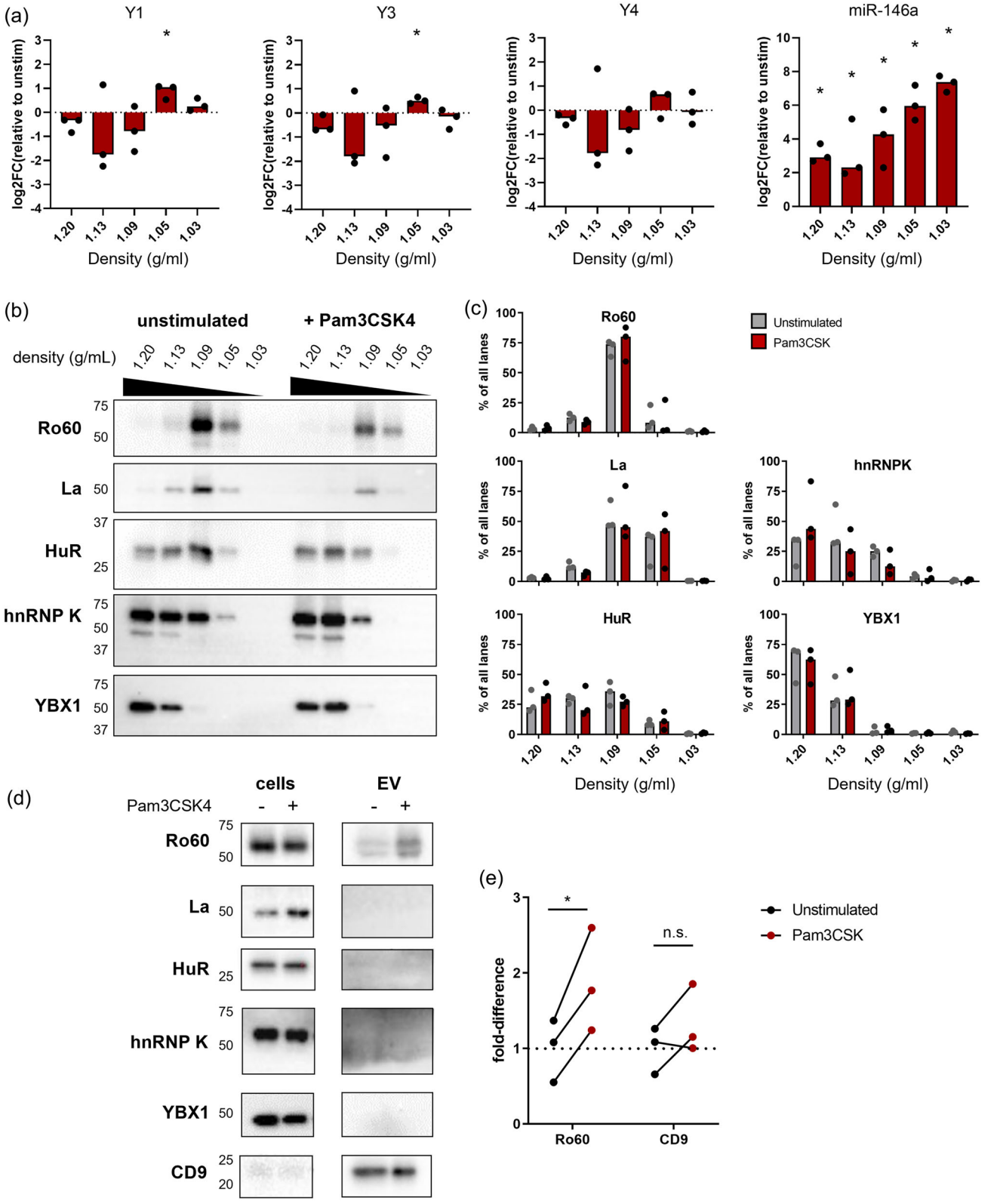

FIGURE 4 Activation of THP-1 macrophages increases local Y RNA levels at (late) endosomal compartments, and increases Ro60 levels in EVs. THP1 cells were stimulated or not with Pam3CSK4, and subjected to subcellular fractionation 4 h after stimulation. (a) Y RNA subtypes and miR-146a in the different subcellular density fractions were quantified by RT-qPCR. For each fraction, we calculated the delta Cq between stimulated and unstimulated conditions (log2 fold change), which are shown in the graph. Deviation from zero ($n = 3$ experiments) was tested by one-sample t test, $^*p < 0.05$ was considered significant. (b) Western blot detection of Y RNA binding proteins in subcellular fractions of Pam3CSK4 stimulated and unstimulated THP1 cells. Blots are representative for $n = 3$ experiments. (c) Quantification of the band intensities in (b). The band intensity per fraction is expressed as percentage of the total band intensity in all lanes of unstimulated or stimulated conditions. Data from $n = 3$ experiments are shown. (d) Western blot detection of Y RNA binding proteins in EVs and cell lysates of Pam3CSK4 stimulated and unstimulated THP1 cells. Loading of cell lysates was normalised to total protein amount, loading of EVs was normalised

(Continues)

FIGURE 4 (Continued)
to EV counts measured by high resolution flow cytometry (Figure 1c). Blots are representative for $n = 3$ experiments. (e) Quantification of EV-assoBiociated Ro60 and CD9 levels on the blots in (b). The fold difference in band intensity was expressed relative to the unstimulated condition. $^*p < 0.05$, Student's paired t test, two tailed, $n = 3$ experiments.

subcellular distribution of Y RNA over different subcellular compartments, we employed fractionation of cytosolic organelles. This method has been frequently used to study changes in protein localisation within cells (Gibbings et al., 2009; Huotari et al., 2012; Matarrese et al., 2008; McKenzie et al., 2016; Santangelo et al., 2016; Squadrito et al., 2014). Relatively few studies have used it to determine the subcellular distribution of ncRNA. These studies mainly focused on miRNA, but not on other ncRNA types such as Y RNA (Gibbings et al., 2009; Squadrito et al., 2014). We observed that Y RNA was highly abundant in (late) endosomal fractions characterised by the presence of Lamp-1, CD63, Tsg101 and EEA1. In contrast, the endotoxin-responsive microRNA miR-146a did not preferentially localise to a specific subcellular fraction (Figure S2C). Importantly, we found that stimulation of cells changed the abundance of Y RNA in the endosomal fractions independent from cytoplasmic Y RNA abundance, and that these changes were reflected by changes in the abundance of Y RNA in EVs. This suggests that the local abundance of Y RNA at these sites may aid its incorporation into EVs. In contrast, miR-146a levels in EVs corresponded with overall changes in miR-146a in all organelle fractions, suggesting incorporation by passive diffusion.

Although co-fractionation of RNA, proteins and organelles does not fully prove their close proximity or physical interaction, our data suggest that the abundance of RNAs at EV biogenesis sites may affect their incorporation into EVs. Similar to our findings, Squadrito et al. showed that overexpression of miR-511-3p increased its abundance in subcellular fractions enriched for EV-marker CD81, which was reflected by increased levels of this miRNA in EVs (Squadrito et al., 2014). Conversely, over-expressing the 3′UTR target sequences for miR-511-3p sequestered this miRNA into P-bodies found in low-density fractions, simultaneously decreasing the levels of this miRNA in EVs (Squadrito et al., 2014). A different study showed that reduced co-fractionation between Ago2 and EV-biogenesis protein Rab7, in cells with mutant oncogene KRAS, resulted in diminished Ago2 and miRNA incorporation into EVs (Cha et al., 2015; McKenzie et al., 2016). These studies support the idea that the local abundance of Y RNA at EV biogenesis sites may contribute to the abundance of this RNA in EVs.

4.2 | Not all previously identified Y RNA binding proteins are detectable in highly purified EV

For our current study, we specifically selected Y RNA binding proteins that were previously detected in EV preparations (Driedonks & Nolte-'t Hoen, 2019). However, only one out of the five tested Y RNA binding proteins was detected in our density gradient purified EVs. This discrepancy may be attributed to differences in EV source and/or purification method. The studies that reported these Y RNA binding proteins in EVs were performed with a variety of biological samples (i.e., seminal fluid (Vojtech et al., 2014)), glioblastoma cells (Wei et al., 2017), bladder cancer cells (Welton et al., 2010), macrophages (Frye et al., 2009), mesenchymal stem cells (Collino et al., 2010) and liver cells (Mukherjee et al., 2016)). EVs from different cell types vary in molecular composition, and may therefore also differ in the type of Y RNA binding proteins they contain. The differences in findings may also be caused by differences in EV isolation protocols. In most previous studies, EVs were isolated by differential centrifugation and successive pelleting by ultracentrifugation. This method enriches for EVs, but additionally co-isolates many non-EV associated proteins (Colombo et al., 2014). To remove these contaminants, we included a density gradient step for EV purification. Previous studies have demonstrated that RBP presumed to be EV-associated, such as YBX1, were absent in density-gradient purified EVs from multiple cell lines (Jeppesen et al., 2019). The same may be the case for other Y RNA binding proteins that were detected in EVs previously, but were non-detectable in our gradient purified EVs.

4.3 | EVs contain Y RNA and Ro60 but not La

Ro60 was the only Y RNA binding protein that was detectable in EVs, and cellular activation led to a parallel increase in the abundance of both Ro60 and Y RNA in EVs. Whether all Y RNA in EVs was associated to Ro60, and whether all Ro60 in EVs was bound to Y RNA remains to be investigated, as the stoichiometry of Y RNA and Ro60 is not fully understood. The absence of La, the other main Y RNA binding protein, in EVs was remarkable since La also aids in the stabilisation of cytoplasmic Y RNA (Labbé et al., 1999; Wolin & Cedervall, 2002; Xue et al., 2003). Interestingly, La shields off the 5′ triphosphate nucleotide of Y RNA (Wolin & Cedervall, 2002), which is a ligand for RIG-I, an innate immune receptor for detection of viral RNA (Hornung et al., 2006). Unshielded triphosphorylated Y RNA can activate RIG-I in recipient cells, which may occur after fusion of EVs with the endosomal membrane or plasma membrane. Whether changes in triphosphorylation of Y RNA plays a role in their release into EVs has not been studied. Although HuR and hnRNP K were not detected in EVs, they were abundant in the cytosolic density

fractions enriched for Y RNA and EV biogenesis markers. It is possible that these proteins deliver Y RNA to EV generating compartments, but are not incorporated into EVs themselves.

4.4 | Application of subcellular fractionation in EV research

Research on sorting of RNA and their binding proteins into EVs has mainly focused on comparing total (cytoplasmic) cellular levels of these molecules of interest to the levels in EVs. However, many RNAs and RBPs are non-equally distributed over the cell and their activity may depend on their localisation to specific cellular compartments (Engel et al., 2020; Turner & Díaz-Muñoz, 2018). This holds true not only for mRNAs, but also for Y RNA and miRNAs (Olejniczak et al., 2015; Tebaldi et al., 2018). Y3 RNA, for example, regulates gene expression by scavenging the enhancer protein HuD away from the mRNAs stabilised by this protein during translation at polysomes (Tebaldi et al., 2018). For EV research, analysis of local intracellular changes in RNA/RBP concentrations is relevant as this is a second parameter besides overall transcriptional levels that can influence sorting of RNAs into EVs. While mRNA can be studied at subcellular resolution via imaging techniques, for example, via aptamer-based approaches (Boersma et al., 2020; Yoon et al., 2016), this is less feasible for many ncRNAs due to their short lengths. Our subcellular fractionation approach enables parallel quantification of ncRNA and proteins, and may be combined with other techniques such as ChIP-seq to further interrogate protein-RNA interactions with subcellular resolution (Gräwe et al., 2021).

5 | CONCLUSION

Y RNAs are abundantly present in EVs and are increasingly identified as biomarker for diseases such as cancer, atherosclerosis and inflammatory conditions (Haderk et al., 2017; Lovisa et al., 2020; Repetto et al., 2015). Our results demonstrate how Y RNAs and their protein interaction partners are distributed over cellular compartments and EVs, and provide insight for further studies on how incorporation of Y RNA into EVs is controlled.

AUTHOR CONTRIBUTIONS

Tom Driedonks: Conceptualization; methodology; investigation; formal analysis; writing—original draft. **Sarah Ressel**: Investigation; writing—review and editing. **Thi Tran Ngoc Minh**: Investigation; writing—review and editing. **Amy Buck**: Supervision; funding acquisition; resources; writing—review and editing. **Esther Nolte-'t Hoen**: Conceptualization; supervision; funding acquisition; writing—original draft; writing—review and editing.

ACKNOWLEDGEMENTS

The authors would like to thank Dr. G.J.A. Arkesteijn for assistance with the high-resolution flow cytometric measurements, and Dr. S.L. Wolin for kindly providing us with the Ro60 antibody. The authors declare no conflicts of interest. This work was supported by FP7 Ideas: European Research Council grant number 337581 to ENMNtH and European Research Council grant number 101002385 to AHB.

CONFLICT OF INTEREST STATEMENT

The authors declare no conflicts of interest.

ORCID

Tom A. P. Driedonks https://orcid.org/0000-0003-0928-9712
Sarah Ressel https://orcid.org/0000-0002-4496-6929
Amy H. Buck https://orcid.org/0000-0003-2645-7191
Esther N. M. Nolte-'t Hoen https://orcid.org/0000-0002-3172-9959

REFERENCES

Akopian, D., Shen, K., Zhang, X., & Shan, S. (2013). Signal Recognition Particle: an essential protein targeting machine. *Annual Review of Biochemistry*, *30*, 311–328. https://doi.org/10.1016/j.cll.2010.01.003.Lyme

Anderson, P., & Ivanov, P. (2014). TRNA fragments in human health and disease. *FEBS Letters*, *588*, 4297–4304. https://doi.org/10.1016/j.febslet.2014.09.001

Bellingham, S. A., Coleman, B. M., & Hill, A. F. (2012). Small RNA deep sequencing reveals a distinct miRNA signature released in exosomes from prion-infected neuronal cells. *Nucleic Acids Research*, *40*, 10937–10949. https://doi.org/10.1093/nar/gks832

Boccitto, M., & Wolin, S. L. (2019). Ro60 and Y RNAs: structure, functions, and roles in autoimmunity. *Critical Reviews in Biochemistry and Molecular Biology*, *54*, 133–152. https://doi.org/10.1080/10409238.2019.1608902

Boersma, S., Rabouw, H. H., Bruurs, L. J. M., Pavlovič, T., van Vliet, A. L. W., Beumer, J., Clevers, H., van Kuppeveld, F. J. M., & Tanenbaum, M. E. (2020). Translation and replication dynamics of single RNA viruses. *Cell*, *183*, 1930–1945.e23. https://doi.org/10.1016/j.cell.2020.10.019

Cha, D. J., Franklin, J. L., Dou, Y., Liu, Q., Higginbotham, J. N., Beckler, M. D., Weaver, A. M., Vickers, K., Prasad, N., Levy, S., Zhang, B., Coffey, R. J., & Patton, J. G. (2015). KRAS-dependent sorting of miRNA to exosomes. *Elife*, *4*, 1–22. https://doi.org/10.7554/eLife.07197

Chen, X., Smith, J. D., Shi, H., Yang, D. D., Flavell, R. A., & Wolin, S. L. (2003). The Ro autoantigen binds misfolded U2 small nuclear RNAs and assists mammalian cell survival after UV irradiation. *Current Biology*, *13*, 2206–2211. https://doi.org/10.1016/j.cub.2003.11.028

Collino, F., Deregibus, M. C., Bruno, S., Sterpone, L., Aghemo, G., Viltono, L., Tetta, C., & Camussi, G. (2010). Microvesicles derived from adult human bone marrow and tissue specific mesenchymal stem cells shuttle selected pattern of miRNAs. *PLoS ONE*, *5*(7), e11803. https://doi.org/10.1371/journal.pone.0011803

Colombo, M., Raposo, G., & Théry, C. (2014). Biogenesis, secretion, and intercellular interactions of exosomes and other extracellular vesicles. *Annual Review of Cell and Developmental Biology*, *30*, 255–289. https://doi.org/10.1146/annurev-cellbio-101512-122326

Crossland, R. E., Norden, J., Bibby, L. A., Davis, J., & Dickinson, A. M. (2016). Evaluation of optimal extracellular vesicle small RNA isolation and qRT-PCR normalisation for serum and urine. *Journal of Immunological Methods*, *429*, 39–49. https://doi.org/10.1016/j.jim.2015.12.011

de Jong, O. G., Murphy, D. E., Mäger, I., Willms, E., Garcia-Guerra, A., Gitz-Francois, J. J., Lefferts, J., Gupta, D., Steenbeek, S. C., van Rheenen, J., El Andaloussi, S., Schiffelers, R. M., Wood, M. J. A., & Vader, P. (2020). A CRISPR-Cas9-based reporter system for single-cell detection of extracellular vesicle-mediated functional transfer of RNA. *Nature Communications*, *11*, 1–13. https://doi.org/10.1038/s41467-020-14977-8

Dhahbi, J. M., Spindler, S. R., Atamna, H., Boffelli, D., Mote, P., & Martin, D. I. K. (2013). 5'-YRNA fragments derived by processing of transcripts from specific YRNA genes and pseudogenes are abundant in human serum and plasma. *Physiological Genomics*, *45*, 990–998. https://doi.org/10.1152/physiolgenomics.00129.2013

Driedonks, T. A. P., Mol, S., de Bruin, S., Peters, A. L., Zhang, X. G., Lindenbergh, M. F. S., Beuger, B. M., van Stalborch, A. D., Spaan, T., de Jong, E. C., van der Vries, E., Margadant, C., van Bruggen, R., Vlaar, A. P. J., Groot Kormelink, T., & Nolte-'t Hoen, E. N. M. (2020). Y-RNA subtype ratios in plasma extracellular vesicles are cell type- specific and are candidate biomarkers for inflammatory diseases. *Journal of Extracellular Vesicles*, *9*, 1764213, https://doi.org/10.1080/20013078.2020.1764213

Driedonks, T. A. P., Nijen-Twilhaar, M. K., & Nolte-'t Hoen, E. N. M. (2018). Technical approaches to reduce interference of Fetal calf serum derived RNA in the analysis of extracellular vesicle RNA from cultured cells. *Journal of Extracellular Vesicles*, *8*, 1552059. https://doi.org/10.1080/20013078.2018.1552059

Driedonks, T. A. P., & Nolte-'t Hoen, E. N. M. (2019). Circulating Y-RNAs in extracellular vesicles and ribonucleoprotein complexes; implications for the immune system. *Frontiers in Immunology*, *9*, 1–15. https://doi.org/10.3389/fimmu.2018.03164

Driedonks, T. A. P., van der Grein, S. G., Ariyurek, Y., Buermans, H. P. J., Jekel, H., Chow, F. W. N., Wauben, M. H. M., Buck, A. H., & Hoen, P. A. C. (2018). Nolte-'t Hoen ENM. Immune stimuli shape the small noncoding transcriptome of extracellular vesicles released by dendritic cells. *Cellular and Molecular Life Sciences*, *75*, 3857–3875. https://doi.org/10.1007/s00018-018-2842-8

Engel, K. L., Arora, A., Goering, R., Lo, H. Y. G., & Taliaferro, J. M. (2020). Mechanisms and consequences of subcellular RNA localization across diverse cell types. *Traffic*, *21*, 404–418. https://doi.org/10.1111/tra.12730

Fabini, G., Raijmakers, R., Hayer, S., Fouraux, M. A., Pruijn, G. J. M., & Steiner, G. (2001). The heterogeneous nuclear ribonucleoproteins I and K interact with a subset of the Ro ribonucleoprotein-associated Y RNAs in vitro and in vivo. *Journal of Biological Chemistry*, *276*, 20711–20718. https://doi.org/10.1074/jbc.M101360200

Farris, A. D., Puvion-Dutilleul, F., Puvion, E., Harley, J. B., & Lee, L. A. (1997). The ultrastructural localization of 60-kDa Ro protein and human cytoplasmic RNAs: Association with novel electron-dense bodies. *Proceedings of the National Academy of Sciences of the United States of America*, *94*, 3040–3045. https://doi.org/10.1073/pnas.94.7.3040

Frye, B. C., Halfter, S., Djudjaj, S., Muehlenberg, P., Weber, S., Raffetseder, U., En-Nia, A., Knott, H., Baron, J. M., Dooley, S., Bernhagen, J., & Mertens, P. R. (2009). Y-box protein-1 is actively secreted through a non-classical pathway and acts as an extracellular mitogen. *EMBO Reports*, *10*, 783–789. https://doi.org/10.1038/embor.2009.81

Fuchs, G., Stein, A. J., Fu, C., Reinisch, K. M., & Wolin, S. L. (2006). Structural and biochemical basis for misfolded RNA recognition by the Ro autoantigen. *Nature Structural and Molecular Biology*, *13*, 1002–1009. https://doi.org/10.1038/nsmb1156

Gámbaro, F., Li Calzi, M., Fagúndez, P., Costa, B., Greif, G., Mallick, E., Lyons, S., Ivanov, P., Witwer, K., Cayota, A., & Tosar, J. P. (2019). Stable tRNA halves can be sorted into extracellular vesicles and delivered to recipient cells in a concentration-dependent manner. *RNA Biology*, *00*, 1–15. https://doi.org/10.1080/15476286.2019.1708548

Gibbings, D. J. (2011). Continuous density gradients to study Argonaute and GW182 complexes associated with the endocytic pathway. *Methods in Molecular Biology*, *725*, 63–76. https://link.springer.com/protocol/10.1007/978-1-61779-046-1_5

Gibbings, D. J., Ciaudo, C., Erhardt, M., & Voinnet, O. (2009). Multivesicular bodies associate with components of miRNA effector complexes and modulate miRNA activity. *Nature Cell Biology*, *11*, 1143–1149. https://doi.org/10.1038/ncb1929

Gräwe, C., Stelloo, S., van Hout, F. A. H., & Vermeulen, M. (2021). RNA-centric methods: Toward the interactome of specific RNA transcripts. *Trends in Biotechnology*, *39*, 890–900. https://doi.org/10.1016/j.tibtech.2020.11.011

Groot Kormelink, T., Arkesteijn, G. J. A., Nauwelaers, F. A., van den Engh, G., Nolte-'t Hoen, E. N. M., & Wauben, M. H. M. (2016). Prerequisites for the analysis and sorting of extracellular vesicle subpopulations by high-resolution flow cytometry. *Cytometry Part A*, *89*, 135–147. https://doi.org/10.1002/cyto.a.22644

Haderk, F., Schulz, R., Iskar, M., Cid, L. L., Worst, T., Willmund, K. V., Schulz, A., Warnken, U., Seiler, J., Benner, A., Nessling, M., Zenz, T., Göbel, M., Dürig, J., Diederichs, S., Paggetti, J., Moussay, E., Stilgenbauer, S., Zapatka, M., … Lichter, P. (2017). Tumor-derived exosomes modulate PD-L1 expression in monocytes. *Science Immunology*, *2*, eaah5509. https://doi.org/10.1126/sciimmunol.aah5509

He, L., & Hannon, G. J. (2004). MicroRNAs: small RNAs with a big role in gene regulation. *Nature Reviews Genetics*, *5*, 522–531. https://doi.org/10.1038/nrg1379

Hornung, V., Ellegast, J., Kim, S., Brzózka, K., Jung, A., Kato, H., Poeck, H., Akira, S., Conzelmann, K.-K., Schlee, M., Endres, S., & Hartmann, G. (2006). 5'-Triphosphate RNA is the Ligand for RIG-I. *Science*, *314*, 994–997. https://doi.org/10.1126/science.1132505

Huotari, J., & Helenius, A. (2011). Endosome maturation. *The EMBO Journal*, *30*, 3481–3500. https://doi.org/10.1038/emboj.2011.286

Huotari, J., Meyer-Schaller, N., Hubner, M., Stauffer, S., Katheder, N., Horvath, P., Mancini, R., Helenius, A., & Peter, M. (2012). Cullin-3 regulates late endosome maturation. *Proceedings of the National Academy of Sciences*, *109*, 823–828. https://doi.org/10.1073/pnas.1118744109

Jeppesen, D. K., Fenix, A. M., Franklin, J. L., Higginbotham, J. N., Zhang, Q., Zimmerman, L. J., Liebler, D. C., Ping, J., Liu, Q., Evans, R., Fissell, W. H., Patton, J. G., Rome, L. H., Burnette, D. T., & Coffey, R. J. (2019). Reassessment of exosome composition. *Cell*, *177*, 428–445.e18. https://doi.org/10.1016/j.cell.2019.02.029

Kobayashi, T., Vischer, U. M., Rosnoblet, C., Lebrand, C., Lindsay, M., Parton, R. G., Kruithof, E. K. O., & Gruenberg, J. (2013). The tetraspanin CD63/lamp3 cycles between endocytic and secretory compartments in human endothelial cells. *Molecular Biology of the Cell*, *11*, 1829–1843. https://doi.org/10.1091/mbc.11.5.1829

Köhn, M., Ihling, C., Sinz, A., Krohn, K., & Hüttelmaier, S. (2015). The Y3** ncRNA promotes the 3′ end processing of histone mRNAs. *Genes and Development*, *29*, 1998–2003. https://doi.org/10.1101/gad.266486.115

Labbé, J. C., Hekimi, S., & Rokeach, L. A. (1999). The levels of the RoRNP-associated Y RNA are dependent upon the presence of ROP-1, the *Caenorhabditis elegans* Ro60 protein. *Genetics*, *151*, 143–150.

Lässer, C., Shelke, G. V., Yeri, A., Kim, D.-K., Crescitelli, R., Raimondo, S., Sjöstrand, M., Gho, Y. S., Van Keuren Jensen, K., & Lötvall, J. (2017). Two distinct extracellular RNA signatures released by a single cell type identified by microarray and next-generation sequencing. *RNA Biology*, *14*, 58–72. https://doi.org/10.1080/15476286.2016.1249092

Lee, H., Li, C., Zhang, Y., Zhang, D., Otterbein, L. E., & Jin, Y. (2019). Caveolin-1 selectively regulates microRNA sorting into microvesicles after noxious stimuli. *Journal of Experimental Medicine*, *216*, 2202–2220.

Leng, Y., Sim, S., Magidson, V., & Wolin, S. L. (2020). Noncoding Y RNAs regulate the levels, subcellular distribution and protein interactions of their Ro60 autoantigen partner. *Nucleic Acids Research*, *48*(12), 6919–6930. https://doi.org/10.1093/nar/gkaa414

Liu, J.-L., & Gall, J. G. (2007). U bodies are cytoplasmic structures that contain uridine-rich small nuclear ribonucleoproteins and associate with P bodies. *Proceedings of the National Academy of Sciences*, *104*, 11655–11659. https://doi.org/10.1073/pnas.0704977104

Lovisa, F., Di Battista, P., Gaffo, E., Damanti, C. C., Garbin, A., Gallingani, I., Carraro, E., Pillon, M., Biffi, A., Bortoluzzi, S., & Mussolin, L. (2020). RNY4 in circulating exosomes of patients with pediatric anaplastic large cell lymphoma: An active player? *Frontiers in Oncology*, *10*, 1–8. https://doi.org/10.3389/fonc.2020.00238

Mann, M., Mehta, A., Zhao, J. L., Lee, K., Marinov, G. K., Garcia-Flores, Y., & Baltimore, D. (2017). An NF-κB-microRNA regulatory network tunes macrophage inflammatory responses. *Nature Communications*, *8*, 851. https://doi.org/10.1038/s41467-017-00972-z

Matarrese, P., Manganelli, V., Garofalo, T., Tinari, A., Gambardella, L., Ndebele, K., Khosravi-Far, R., Sorice, M., Esposti, M. D., & Malorni, W. (2008). Endosomal compartment contributes to the propagation of CD95/Fas-mediated signals in type II cells. *The Biochemical Journal*, *413*, 467–478. https://doi.org/10.1042/BJ20071704

Mateescu, B., Kowal, E. J. K., van Balkom, B. W. M., Bartel, S., Bhattacharyya, S. N., Buzás, E. I., Buck, A. H., de Candia, P., Chow, F. W. N., Das, S., Driedonks, T. A., Fernández-Messina, L., Haderk, F., Hill, A. F., Jones, J. C., Van Keuren-Jensen, K. R., Lai, C. P., Lässer, C., Liegro, I. D., … Lunavat, T. R. (2017). Obstacles and opportunities in the functional analysis of extracellular vesicle RNA—An ISEV position paper. *Journal of Extracellular Vesicles*, *6*, 1286095. https://doi.org/10.1080/20013078.2017.1286095

Matera, A. G., Frey, M. R., Margelot, K., & Wolin, S. L. (1995). A perinucleolar compartment contains several RNA polymerase III transcripts as well as the polypydmidine tract-binding protein, hnRNP I. *Journal of Cell Biology*, *129*, 1181–1193.

Matera, A. G., & Wang, Z. (2014). A day in the life of the spliceosome. *Nature Reviews: Molecular Cell Biology*, *15*, 108–121. https://doi.org/10.1038/nrm3742

McKenzie, A. J., Hoshino, D., Hong, N. H., Cha, D. J., Franklin, J. L., Coffey, R. J., Patton, J. G., & Weaver, A. M. (2016). KRAS-MEK Signaling Controls Ago2 Sorting into Exosomes. *Cell Reports*, *15*, 978–987. https://doi.org/10.1016/j.celrep.2016.03.085

Mosbach, M. L., Pfafenrot, C., von Strandmann, E. P., Bindereif, A., & Preußer, C. (2021). Molecular determinants for RNA release into extracellular vesicles. *Cells*, *10*, https://doi.org/10.3390/cells10102674

Mukherjee, K., Ghoshal, B., Ghosh, S., Chakrabarty, Y., Shwetha, S., Das, S., & Bhattacharyya, S. N. (2016). Reversible HuR-microRNA binding controls extracellular export of miR122 and augments stress response. *EMBO Reports*, *17*, 11841203. https://doi.org/10.15252/embr

Nolte-'t Hoen, E. N. M., Buermans, H. P. J., Waasdorp, M., Stoorvogel, W., Wauben, M. H. M., & 't Hoen, P. A. C. (2012). Deep sequencing of RNA from immune cell-derived vesicles uncovers the selective incorporation of small non-coding RNA biotypes with potential regulatory functions. *Nucleic Acids Research*, *40*, 9272–9285. https://doi.org/10.1093/nar/gks658

Nolte-'t Hoen, E. N. M., van der Vlist, E. J., Aalberts, M., Mertens, H. C. H., Bosch, B. J., Bartelink, W., Mastrobattista, E., van Gaal, E. V. B., Stoorvogel, W., Arkesteijn, G. J. A., & Wauben, M. H. (2012). Quantitative and qualitative flow cytometric analysis of nanosized cell-derived membrane vesicles. *Nanomedicine : Nanotechnology, Biology, and Medicine*, *8*, 712–720. https://doi.org/10.1016/j.nano.2011.09.006

La Rocca G, Olejniczak, S. H., González, A. J., Briskin, D., Vidigal, J. A., Spraggon, L., DeMatteo, R. G., Radler, M. R., Lindsten, T., Ventura, A., Tuschl, T., Leslie, C. S., & Thompson, C. B. (2015). In vivo, Argonaute-bound microRNAs exist predominantly in a reservoir of low molecular weight complexes not associated with mRNA. *Proceedings of the National Academy of Sciences of the United States of America*, *112*, 767–772. https://doi.org/10.1073/pnas.1424217112

Pall, G. S., & Hamilton, A. J. (2008). Improved northern blot method for enhanced detection of small RNA. *Nature Protocols*, *3*, 1077–1084. https://doi.org/10.1038/nprot.2008.67

Pruijn, G. J. M., Wingens, P., Peters, S. L. M., Thijssen, J. P. H., & Van Venrooij, W. J. (1993). Ro RNP associated Y RNAs are highly conserved among mammals. *Biochimica et Biophysica Acta—Gene Structure and Expression*, *1216*, 395–401. https://doi.org/10.1016/0167-4781(93)90006-Y

Repetto, E., Lichtenstein, L., Hizir, Z., Tekaya, N., Benahmed, M., Ruidavets, J.-B., Zaragosi, L.-E., Perret, B., Bouchareychas, L., Genoux, A., Lotte, R., Ruimy, R., Ferrières, J., Barbry, P., Martinez, L. O., & Trabucchi, M. (2015). RNY-derived small RNAs as a signature of coronary artery disease. *BMC Medicine*, *13*, 259. https://doi.org/10.1186/s12916-015-0489-y

Ridder, K., Sevko, A., Heide, J., Dams, M., Rupp, A.-K. K., Macas, J., Starmann, J., Tjwa, M., Plate, K. H., Sültmann, H., Altevogt, P., Umansky, V., & Momma, S. (2015). Extracellular vesicle-mediated transfer of functional RNA in the tumor microenvironment. *OncoImmunology*, *4*, e1008371. https://doi.org/10.1080/2162402X.2015.1008371

Santangelo, L., Giurato, G., Cicchini, C., Montaldo, C., Mancone, C., Tarallo, R., Battistelli, C., Alonzi, T., Weisz, A., & Tripodi, M. (2016). The RNA-binding protein SYNCRIP is a component of the hepatocyte exosomal machinery controlling microRNA sorting. *Cell Reports*, *17*, 799–808. https://doi.org/10.1016/j.celrep.2016.09.031

Scheckel, C., Drapeau, E., Frias, M. A., Park, C. Y., Fak, J., Zucker-Scharff, I., Kou, Y., Haroutunian, V., Ma'ayan, A., Buxbaum, J. D., & Darnell, R. B. (2016). Regulatory consequences of neuronal ELAV-like protein binding to coding and non-coding RNAs in human brain. *Elife*, *5*, 1–35. https://doi.org/10.7554/eLife.10421

Shurtleff, M. J., Temoche-Diaz, M. M., Karfilis, K V., Ri, S., & Schekman, R. (2016). Y-box protein 1 is required to sort microRNAs into exosomes in cells and in a cell-free reaction. *Elife*, *5*, 1–23. https://doi.org/10.7554/eLife.19276

Shurtleff, M. J., Yao, J., Qin, Y., Nottingham, R. M., Temoche-Diaz, M. M., Schekman, R., & Lambowitz, A. M. (2017). A broad role for YBX1 in defining the small non-coding RNA composition of exosomes. *Proceedings of the National Academy of Sciences of the United States of America*, *114*, 8987–8995. https://doi.org/10.1073/pnas.1712108114

Sim, S., Weinberg, D. E., Fuchs, G., Choi, K., Chung, J., & Wolin, S. L. (2009). The subcellular distribution of an RNA quality control protein, the Ro autoantigen, is regulated by noncoding Y RNA binding. *Molecular Biology of the Cell*, *20*, 1555–1564. https://doi.org/10.1091/mbc.E08

Sim, S., Yao, J., Weinberg, D. E., Niessen, S., Yates, J. R., & Wolin, S. L. (2012). The zipcode-binding protein ZBP1 influences the subcellular location of the Ro 60-kDa autoantigen and the noncoding Y3 RNA. *RNA (New York, NY)*, *18*, 100–110. https://doi.org/10.1261/rna.029207.111

Simons, F. H. M., Rutjes, S. A., Van Venrooij, W. J., & Pruijn, G. J. M. (1996). The interactions with Ro60 and La differentially affect nuclear export of hY1 RNA. *RNA*, *2*, 264–273.

Squadrito, M. L., Baer, C., Burdet, F., Maderna, C., Gilfillan, G. D., Lyle, R., Ibberson, M., & De Palma, M. (2014). Endogenous RNAs modulate microRNA sorting to exosomes and transfer to acceptor cells. *Cell Reports*, *8*, 1432–1446. https://doi.org/10.1016/j.celrep.2014.07.035

Statello, L., Maugeri, M., Garre, E., Nawaz, M., Wahlgren, J., Papadimitriou, A., Lundqvist, C., Lindfors, L., Colle, A., Sunnerhagen, P., Ragusa, M., Purrello, M., Di Pietro, C., Tigue, N., & Valadi, H. (2018). Identification of RNA-binding proteins in exosomes capable of interacting with different types of RNA: RBP-facilitated transport of RNAs into exosomes. *PLoS One*, *13*, 1–30. https://doi.org/10.1371/journal.pone.0195969

Stein, A. J., Fuchs, G., Fu, C., Wolin, S. L., & Reinisch, K. M. (2005). Structural insights into RNA quality control: The Ro autoantigen binds misfolded RNAs via its central cavity. *Cell*, *121*, 529–539. https://doi.org/10.1016/j.cell.2005.03.009

Taganov, K. D., Boldin, M. P., Chang, K. J., & Baltimore, D. (2006). NF-κB-dependent induction of microRNA miR-146, an inhibitor targeted to signaling proteins of innate immune responses. *Proceedings of the National Academy of Sciences of the United States of America*, *103*, 12481–12486. https://doi.org/10.1073/pnas.0605298103

Tebaldi, T., Zuccotti, P., Peroni, D., Köhn, M., Gasperini, L., Potrich, V., Bonazza, V., Dudnakova, T., Rossi, A., Sanguinetti, G., Conti, L., Macchi, P., D'Agostino, V., Viero, G., Tollervey, D., Hüttelmaier, S., & Quattrone, A. (2018). HuD is a neural translation enhancer acting on mTORC1-responsive genes and counteracted by the Y3 small non-coding RNA. *Molecular Cell*, *71*, 256–270. https://doi.org/10.1016/j.molcel.2018.06.032

Temoche-Diaz, M. M., Shurtleff, M. J., Nottingham, R. M., Yao, J., Fadadu, R. P., Lambowitz, A. M., & Schekman, R. (2019). Distinct mechanisms of microRNA sorting into cancer cell-derived extracellular vesicle subtypes. *Elife*, *8*, 1–34. https://doi.org/10.1192/bjp.111.479.1009-a

Tosar, J. P., Gambaro, F., Sanguinetti, J., Bonilla, B., Witwer, K. W., & Cayota, A. (2015). Assessment of small RNA sorting into different extracellular fractions revealed by high-throughput sequencing of breast cell lines. *Nucleic Acids Research*, *43*(11), 5601–5616. https://doi.org/10.1093/nar/gkv432

Turner, M., & Díaz-Muñoz, M. D. (2018). RNA-binding proteins control gene expression and cell fate in the immune system. *Nature Immunology*, *19*, 120–129. https://doi.org/10.1038/s41590-017-0028-4

Valadi, H., Ekström, K., Bossios, A., Sjöstrand, M., Lee, J. J., & Lötvall, J. O. (2007). Exosome-mediated transfer of mRNAs and microRNAs is a novel mechanism of genetic exchange between cells. *Nature Cell Biology*, *9*, 654–659. https://doi.org/10.1038/ncb1596

van der Vlist, E. J., Nolte-'t Hoen, E. N. M., Stoorvogel, W., Arkesteijn, G. J. A., & Wauben, M. H. M. (2012). Fluorescent labeling of nano-sized vesicles released by cells and subsequent quantitative and qualitative analysis by high-resolution flow cytometry. *Nature Protocols*, *7*, 1311–1326. https://doi.org/10.1038/nprot.2012.065

Van Deun, J., Mestdagh, P., Agostinis, P., Akay, Ö., Anand, S., Anckaert, J., Martinez, Z. A., Baetens, T., Beghein, E., Bertier, L., Berx, G., Boere, J., Boukouris, S., Bremer, M., Buschmann, D., Byrd, J. B., Casert, C., Cheng, L., Cmoch, A., … Hendrix, A. (2017). EV-TRACK: Transparent reporting and centralizing knowledge in extracellular vesicle research. *Nature Methods*, *14*, 228–232. https://doi.org/10.1038/nmeth.4185

van Helden, S. F. G., van Leeuwen, F. N., & Figdor, C. G. (2008). Human and murine model cell lines for dendritic cell biology evaluated. *Immunology Letters*, *117*, 191–197. https://doi.org/10.1016/j.imlet.2008.02.003

van Niel, G., D'Angelo, G., & Raposo, G. (2018). Shedding light on the cell biology of extracellular vesicles. *Nature Reviews Molecular Cell Biology*, *19*, 213–228. https://doi.org/10.1038/nrm.2017.125

Villarroya-Beltri, C., Gutiérrez-Vázquez, C., Sánchez-Cabo, F., Pérez-Hernández, D., Vázquez, J., Martin-Cofreces, N., Martinez-Herrera, D. J., Pascual-Montano, A., Mittelbrunn, M., & Sánchez-Madrid, F. (2013). Sumoylated hnRNPA2B1 controls the sorting of miRNAs into exosomes through binding to specific motifs. *Nature Communications*, *4*, 2980. https://doi.org/10.1038/ncomms3980

Vojtech, L., Woo, S., Hughes, S., Levy, C., Ballweber, L., Sauteraud, R. P., Strobl, J., Westerberg, K., Gottardo, R., Tewari, M., & Hladik, F. (2014). Exosomes in human semen carry a distinctive repertoire of small non-coding RNAs with potential regulatory functions. *Nucleic Acids Research*, *42*, 7290–7304. https://doi.org/10.1093/nar/gku347

Wei, Z., Batagov, A. O., Schinelli, S., Wang, J., Wang, Y., El Fatimy, R., Rabinovsky, R., Balaj, L., Chen, C. C., Hochberg, F., Carter, B., Breakefield, X. O., & Krichevsky, A. M. (2017). Coding and noncoding landscape of extracellular RNA released by human glioma stem cells. *Nature Communications*, *8*, 1145. https://doi.org/10.1038/s41467-017-01196-x

Welton, J. L., Khanna, S., Giles, P. J., Brennan, P., Brewis, I. A., Staffurth, J., Mason, M. D., & Clayton, A. (2010). Proteomics analysis of bladder cancer exosomes. *Molecular & Cellular Proteomics*, *9*, 1324–1338. https://doi.org/10.1074/mcp.M000063-MCP201

Wolin, S. L., & Cedervall, T. (2002). The La Protein. *Annual Review of Biochemistry*, *71*, 375–403. https://doi.org/10.1146/annurev.biochem.Copyright

Xue, D., Shi, H., Smith, J. D., Chen, X., Noe, D. A., Cedervall, T., Yang, D. D., Eynon, E., Brash, D. E., Kashgarian, M., Flavell, R. A., & Wolin, S. L. (2003). A lupus-like syndrome develops in mice lacking the Ro 60-kDa protein, a major lupus autoantigen. *Proceedings of the National Academy of Sciences of the United States of America*, *100*, 7503–7508. https://doi.org/10.1073/pnas.0832411100

Yoon, Y. J., Wu, B., Buxbaum, A. R., Das, S., Tsai, A., English, B. P., Grimm, J. B., Lavis, L. D., & Singer, R. H. (2016). Glutamate-induced RNA localization and translation in neurons. *Proceedings of the National Academy of Sciences of the United States of America*, *113*, E6877–E6886. https://doi.org/10.1073/pnas.1614267113

Zietzer, A., Hosen, M. R., Wang, H., Goody, P. R., Sylvester, M., Latz, E., Nickenig, G., Werner, N., & Jansen, F. (2020). The RNA-binding protein hnRNPU regulates the sorting of microRNA-30c-5p into large extracellular vesicles. *Journal of Extracellular Vesicles*, *9*, 1786967. https://doi.org/10.1080/20013078.2020.1786967

Zomer, A., Maynard, C., Verweij, F. J., Kamermans, A., Schäfer, R., Beerling, E., Schiffelers, R. M., de Wit, E., Berenguer, J., Ellenbroek, S. I. J., Wurdinger, T., Pegtel, D. M., & van Rheenen, J. (2015). In vivo imaging reveals extracellular vesicle-mediated phenocopying of metastatic behavior. *Cell*, *161*, 1046–1057. https://doi.org/10.1016/j.cell.2015.04.042

SUPPORTING INFORMATION

Additional supporting information can be found online in the Supporting Information section at the end of this article.

How to cite this article: Driedonks, T. A. P., Ressel, S., Tran Ngoc Minh, T., Buck, A. H., & Nolte-'t Hoen, E. N. M. (2024). Intracellular localisation and extracellular release of Y RNA and Y RNA binding proteins. *Journal of Extracellular Biology*, *3*, e123. https://doi.org/10.1002/jex2.123